Chemical Science

ROYAL SOCIETY OF CHEMISTRY

EDGE ARTICLE

View Article Online
View Journal | View Issue



Cite this: *Chem. Sci.*, 2021, **12**, 4014

All publication charges for this article have been paid for by the Royal Society of Chemistry

Received 6th January 2021
Accepted 23rd January 2021

DOI: 10.1039/d1sc00080b

rsc.li/chemical-science

# To improve the key properties of nonlinear optical crystals assembled with tetrahedral functional building units†

Zhiyong Bai, [ad] Lehui Liu, [a] Dongmei Wang,[a] Chun-Li Hu*[b] and Zhoubin Lin *[abc]

Nonlinear optical (NLO) crystals assembled with conventional non-π-conjugated tetrahedral functional building units (FBUs), generally referring to [$PO_4$] and [$BO_4$], usually exhibit weak nonlinearity and poor birefringence. It is currently proposed that partially substituting oxygen atoms with fluoride atoms in these FBUs could enhance these crucial properties. Hence, we investigated for the first time the NLO-related properties of $NH_4BAsO_4F$ (ABAF), which was constructed from tetrahedral [$BO_3F$] and [$AsO_4$] FBUs, and enhancements of these properties were observed in this material, that is large second-harmonic generation (SHG) response (2 × KDP) and improved birefringence (0.03 at 1064 nm). Notably, both SHG coefficient and birefringence of ABAF exceeded those of a great majority of phosphates, sulfates, or boron phosphates and achieved a preferable balance. It is interesting that ABAF shows vast structural similarities to the typical NLO crystals $Sr_2Be_2B_2O_7$ (SBBO) and $KBe_2BO_3F_2$ (KBBF), which might be the partial reason why it showed improvement in these vital properties. This work may afford some inspiration for enhancing the key performances of NLO crystals assembled with non-π-conjugated tetrahedra.



## Introduction

Nonlinear optical (NLO) crystals capable of switching specific coherent light sources generated by a solid-state laser to the ultraviolet (UV) and deep-UV spectral region are of great demand and have attracted considerable attention for their important applications in areas as diverse as photolithography, laser micromachining, and advanced instruments.[1–6] To date, $KBe_2BO_3F_2$ (KBBF) is the sole NLO material that can output the deep-UV coherent radiation by a direct SHG process. However, the practical application was restricted by its intrinsic drawbacks including toxic BeO and layered growth habit.[7]

To be deep-UV NLO candidates, materials must satisfy three fundamental requirements: (1) a short absorption edge, less than 200 nm; (2) large SHG coefficient, >0.39 pm $V^{-1}$; and (3) sufficient birefringence (0.05–0.10).[8–10] It is widely agreed that tetrahedral FBUs, mainly referring to [$PO_4$] and [$BO_4$] tetrahedra, are very helpful for deep-UV transmittance, and thus they have been employed to design and synthesize deep-UV NLO materials.[11] The unremitting efforts by researchers result in a series of NLO-active optical materials exclusively consisting of [$BO_4$] or/and [$PO_4$] tetrahedrons being discovered, such as $SrB_4O_7$,[12] $BPO_4$,[13] $Ba_3P_3O_{10}X$ (X = Cl, Br),[14] $RbBa_2(PO_3)_5$,[15] $LiM_2PO_4$ (M = Rb, Cs),[16,17] $RbNaMgP_2O_7$,[18] and $M_4Mg_4(P_2O_7)_2$ (M = K, Rb).[19] As reported, these materials are transparent down to the deep-UV spectral region very well with a short absorption edge, *e.g.*, $BPO_4$ (130 nm),[13] $Ba_3P_3O_{10}Cl$ (180 nm),[14] $LiCs_2PO_4$ (174 nm),[16] and $K_4Mg_4(P_2O_7)_2$ (170 nm).[19] However, there also remain undesired issues that are often-weak SHG susceptibility and poor birefringence, especially the poor birefringence which vastly limits the phase-matched wavelengths reaching the deep-UV region.[20] In fact, the recent research studies reveal that the SHG coefficient can be efficiently improved by adopting some strategies. For example, the edge-sharing tetrahedra make $LiCs_2PO_4$ and $Li_2BaSiO_4$ exhibit enlarged SHG response of 2.6 and 2.8 times that of KDP, respectively, which are even larger than that of many borate-based NLO crystals.[16,21] Nonetheless, except for a few exceptions, most of these materials have a weak SHG response. Compared to SHG efficiency, improving the

[a]*CAS Key Laboratory of Optoelectronic Materials Chemistry and Physics, Fujian Institute of Research on the Structure of Matter, Chinese Academy of Sciences, Fuzhou, Fujian 350002, P. R. China. E-mail: lzb@fjirsm.ac.cn*

[b]*State Key Laboratory of Structural Chemistry, Fujian Institute of Research on the Structure of Matter, Chinese Academy of Sciences, Fuzhou, Fujian 350002, P. R. China. E-mail: clhu@fjirsm.ac.cn*

[c]*Fujian Science & Technology Innovation Laboratory for Optoelectronic Information of China, Fuzhou, Fujian, 350108, P. R. China*

[d]*University of Chinese Academy of Sciences, Beijing 100049, P. R. China*

† Electronic supplementary information (ESI) available: Tables of crystal data and structure refinement, fractional atomic coordinates, anisotropic displacement parameters, selected bond lengths and bond angles, figures of EDS, DTA/TG, and DOS, and powder X-ray diffraction patterns. CCDC 2049585. For ESI and crystallographic data in CIF or other electronic format see DOI: 10.1039/d1sc00080b

Table 1 The properties of recently discovered deep-UV transparent NLO crystals assembled with tetrahedral FBUs[a]

| Crystals | PSHG (×KDP) | SHG coefficient (pm $V^{-1}$) | Absorption edge (nm) | Birefringence ($\Delta n$) | Ref. |
|---|---|---|---|---|---|
| $BPO_4$ | 2 | $d_{36} = 0.76$ | 134 | 0.0056 @ 589 nm | 13 |
| $Ba_3P_3O_{10}Cl$ | 0.6 | $d_{ave} = 0.57$ | 180 | 0.030 @ 532 nm | 14 |
| $Ba_3P_3O_{10}Br$ | 0.5 | $d_{ave} = 0.49$ | <200 | 0.024 @ 532 nm | 14 |
| $Ba_5P_6O_{20}$ | 0.8 | N. R. | 167 | N. R. | 29 |
| $RbBa_2(PO_3)_5$ | 1.3 | $d_{11} = 0.066$, $d_{12} = 0.037$, $d_{13} = -0.591$, $d_{15} = 0.007$, $d_{24} = 0.197$, $d_{33} = 0.037$ | 163 | 0.009 @ 1064 nm | 15 and 30 |
| $KBa_2(PO_3)_5$ | 0.9 | $d = 7.50$–$7.79 \times 10^{-10}$ esu | 167 | N. R. | 31 |
| $KPb_2(PO_3)_5$ | 0.5 | N. R. | 177 | 0.021 @ 1064 nm | 30 |
| $KLa(PO_3)_4$ | 0.9 | $d_{14} = 1.62 \times 10^{-9}$, $d_{16} = 1.58 \times 10^{-9}$, $d_{22} = d_{23} = 1.65 \times 10^{-9}$ esu | 162 | 0.0084 @ 1064 nm | 32 |
| $K_4Mg_4(P_2O_7)_3$ | 1.3 | N. R. | 170 | 0.0108 @ 1064 nm | 19 |
| $Rb_4Mg_4(P_2O_7)_3$ | 1.4 | N. R. | <200 | 0.009 @ 1064 nm | 19 |
| $RbNaMgP_2O_7$ | 1.5 | N. R. | 185 | N. R. | 18 |
| $CsNaMgP_2O_7$ | 1.1 | $d_{31} = 0.368$, $d_{32} = -0.178$, $d_{33} = -0.321$ | 180 | N. R. | 33 |
| $LiCs_2PO_4$ | 2.6 | $d_{15} = d_{31} = -0.65$, $d_{24} = d_{32} = 0.22$, $d_{33} = 0.61$ | 174 | N. R. | 16 |
| $LiRb_2PO_4$ | 2.1 | $d_{15} = -0.46$, $d_{24} = 0.11$, $d_{33} = 0.28$ | 170 | N. R. | 17 |
| $KBPO_4F$ | 1 | N. R. | <200 | 0.044 | 34 |
| $CsLiCdP_2O_7$ | 1.5 | N. R. | <200 | N. R. | 35 |
| $Ba_2NaClP_2O_7$ | 1.3 | $d_{ave} = 1.11$ | <176 | 0.017 @ 1064 nm | 36 |
| $(NH_4)_2PO_3F$ | 1 | $d_{15} = 0.14$, $d_{24} = 0.40$, $d_{33} = -0.35$, $d_{14} = 0.08$ | <177 | 0.027 @ 1064 nm | 20 |
| $K_2SrP_4O_{12}$ | 0.5 | $d_{14} = -0.534$, $d_{36} = 0.185$ | <200 | 0.016 @ 1064 nm | 37 |
| $KMg(H_2O)PO_4$ | 1.14 | $d_{31} = 0.55$, $d_{32} = 0.48$, $d_{33} = 1.17$ | <200 | 0.018 @ 1064 nm | 38 |
| $NH_4NaPO_3F \cdot H_2O$ | 1.1 | $d_{11} = 0.727$ | N. R. | 0.053 @ 589.3 nm | 23 |
| $NH_4NaLi_2(SO_4)_2$ | 1.1 | N. R. | 186 | N. R. | 39 |
| $Li_2BaSiO_4$ | 2.8 | $d_{15} = d_{31} = -0.26$, $d_{33} = 3.77$ | <190 | N. R. | 21 |
| $CsSiP_2O_7F$ | 0.7 | $d_{16} = -0.22$, $d_{14} = 0.10$, $d_{25} = 0.34$, $d_{23} = -0.35$ | <190 | 0.009 @ 1064 nm | 40 |
| $NH_4BAsO_4F$ | 2 | $d_{12} = 1.25$ | <200 | 0.03 @ 1064 nm | This work |

[a] N. R.: not reported or not available.

birefringence is much more challenging because of the small anisotropy of $[BO_4]$ and $[PO_4]$.[20] On the basis of our statistics, the birefringence of almost all of the reported deep-UV transparent NLO materials in phosphates and boron phosphates is less than 0.02 which is too small to satisfy the phase-matching conditions in the deep-UV region (see Table 1). To address this, Pan's groups proposed that new tetrahedral FBUs, such as $[BO_3F]$ and $[PO_3F]$ tetrahedra, generated by partially substituting the oxygen atoms with fluoride atoms in $[BO_4]$ and $[PO_4]$, respectively, possess superior optical properties compared to the original ones and these new FBUs can efficiently enhance the birefringence of materials.[20,22] Recent research demonstrated the usefulness of this proposition. For example, very recently reported $(NH_4)_2PO_3F$[20] and $NaNH_4PO_3F \cdot H_2O$,[23] both of them exclusively composed of tetrahedral $[PO_3F]$ units, exhibit enhanced birefringence, that is 0.027 and 0.053, respectively. It should be noted that in particular, $NaNH_4PO_3F \cdot H_2O$ exhibits the largest birefringence among phosphates which enable its shortest phase-matching wavelength reaching the deep-UV region (194 nm). Motivated by these achievements, a fluoroboron arsenate, $NH_4BAsO_4F$ (ABAF),[24] which was assembled with $[BO_3F]$ and $[AsO_4]$ tetrahedra, attracted our attention. As mentioned above, the occurrence of $[BO_3F]$ tetrahedra in this compound may induce an enhanced birefringence and $[AsO_4]$ tetrahedra may help in enhancement of SHG coefficient. In this article, we reported for the first time its linear and nonlinear optical properties and explored the structure–property relationships.

## Results and discussion

### Crystal structure and structural comparison

ABAF crystallizes in a non-centrosymmetric (NCS) and polar space group *Cc* (no. 9). Its asymmetric unit consists of one As, one B, one N, one F and four O atoms. The As atom is tetrahedrally coordinated with oxygen atoms, yielding the deformed $[AsO_4]$ tetrahedron with one shorter As–O bond length 1.632(14) Å and three longer As–O bond lengths ranging from 1.705(12) Å to 1.721(13) Å. The B atom forms a distorted $[BO_3F]$ tetrahedral configuration with a shorter B–F bond length 1.391(19) Å and three longer B–O bond lengths varying from 1.45(2) Å to 1.471 (19) Å. The B–F and B–O bond lengths in ABAF agree well with those of NLO crystals containing $BO_3F$ tetrahedra, which are summarized in Table S9.†

Structurally, three $[BO_3F]$ and three $[AsO_4]$ tetrahedra are linked alternately with two longer B–O (or As–O) bonds to create

ladybird-shaped $[B_3As_3O_{15}F_3]$ functional building units (FBUs). The $[B_3As_3O_{15}F_3]$ FBUs are further connected mutually through another longer B–O (or As–O) bond and then extended in the *a*–*b* plane to build a two-dimensional (2D) honeycomb-like $[BAsO_4F]_\infty$ infinite layer, which stacked along the *c*-axis with $NH_4^+$ cations which are located at the interlayer as charge compensation to complete the three-dimensional framework construction. The terminal F atoms in $[BO_3F]$ and O atoms of the shorter As–O bond in $[AsO_4]$ formed a H-bond network with H atoms in $NH_4^+$ to reinforce the interlayer interactions. The H-bond calculation, realized by PLATON, shows that each $NH_4^+$ is bonded to six oxygen atoms and three fluorine atoms to create a $N–H_4\cdots O_6F_3$ H-bond network with a variety of H···O/F bond distances of 2.05 Å to 2.57 Å. It is widely thought that a H-bond network can efficiently strengthen the interlayer binding in layered crystals.[25,26] Thus, ABAF probably has better crystal growth habit than KBBF along the *c* axis. The calculated bond valences are 4.92 and 3.08 for As and B atoms, respectively, which are in accordance with their normal oxidation states.[27]

It is interesting that ABAF "integrated" somehow the crystal structural characteristics of both SBBO and KBBF. For comparison, their crystal structural representations are graphically illustrated in Fig. 1 and then discussed below. Firstly, FBUs of ABAF and SBBO possess homogeneous ladybird-like 12-membered (12M) ring FBUs. In SBBO, three $[BO_3]$ triangles are linked with three $[BeO_4]$ tetrahedra alternately, yielding the $[B_3Be_3O_{15}]$ ladybird-shaped 12M FBU which can be described as (3Δ + 3T); similarly, the ladybird-shaped 12M ring FBU $[As_3B_3O_{15}F_3]$ in ABAF, which can be described as (3T + 3T), is composed of three $[BO_3F]$ and three $[AsO_4]$ tetrahedra. The size of the 12M ring of SBBO and ABAF is very close; the tiny difference between them is that the ring of SBBO is slightly "thinner" and "higher" than that of ABAF. However, KBBF′s FBU, $[Be_2BO_6F_2]$, composed of one $[BO_3]$ triangle and two $[BeO_3F]$ tetrahedra and can be described as (1Δ + 2T), is a 6-membered ring and is distinct from SBBO and KBBF. Secondly, the likeness between ABAF and KBBF is mainly reflected in their 2D single layer structure. In KBBF and ABAF, the single layers were separated by $K^+$ and $NH_4^+$ cations, respectively. The interlayer distance is 6.38 Å for ABAF which is slightly longer than that of KBBF (6.25 Å).[25] However, the inverse $[BeO_4]$ tetrahedra in adjacent $[Be_3B_3O_{12}]$ layers are connected directly by bridging oxygen atoms, which leads to the $[Be_2B_2O_7]$ double layers in SBBO.

## Linear and nonlinear optical properties

The UV-Vis-NIR diffuse reflectance spectrum was recorded to examine the UV transparency capacity and determine the band gap of ABAF (Fig. 2d). The spectrum implies that ABAF is transparent down to the deep-UV spectral region with 30% reflectance at 200 nm. Additionally, ABAF has a high reflectance, corresponding to high transparency, from 220 to 1000 nm (>75%). On the basis of the Kubelka function, the band gap of ABAF is determined to be 5.9 eV.

Attributable to SHG-favorable structural features, mainly referring to the optimized arrangement of $[BO_3F]$ and $[AsO_4]$ groups in space, ABAF may display an enhanced SHG response. To examine this, the particle size dependent powder second harmonic generation (SHG) response was executed utilizing 1064 nm coherent light as an incident source *via* the method

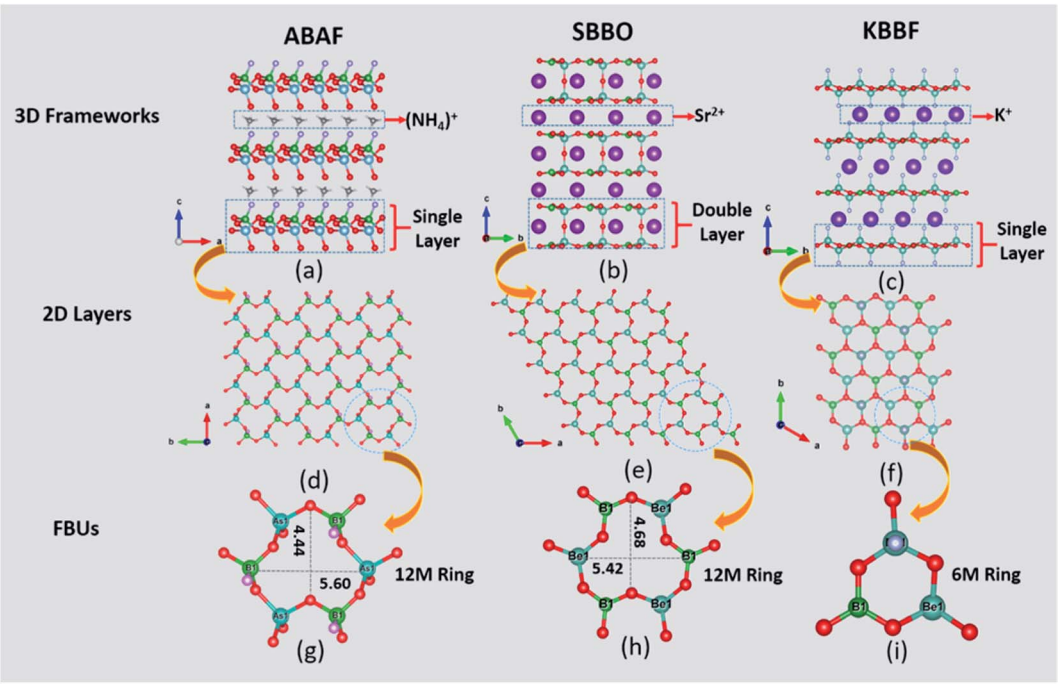


Fig. 1 Crystal structure description of ABAF and structural comparison with SBBO and KBBF. (a)–(c) are the three dimensional frameworks, (d–f) are the two dimensional layers, and (g)–(i) are the FBUs of ABAF, SBBO, and KBBF, respectively.

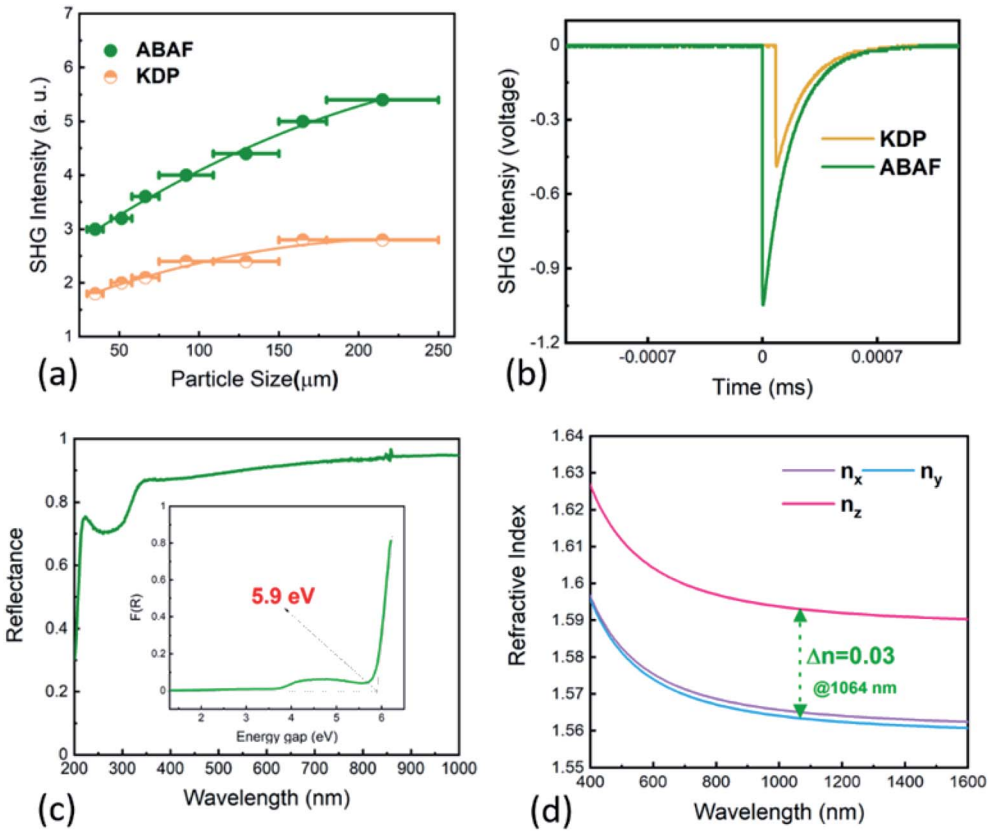


Fig. 2 Nonlinear and linear optical properties of ABAF. (a) Particle size dependent SHG test. (b) SHG signal traces of the oscilloscope. (c) The UV-Vis-NIR reflectance spectrum. (d) Calculated refractive index.

proposed by Kurtz and Perry.[28] $KH_2PO_4$ (KDP) was used as a reference. As is clearly seen from Fig. 2a and b, ABAF exhibits SHG signals, about twice that of KDP in the particle size range of 180–250 μm at 1064 nm. The SHG response of ABAF is superior to or comparable to those deep-UV transparent NLO crystals exclusively composed of nonπ-conjugated tetrahedral FBUs, such as phosphates, sulfates, boron phosphates (see Table 1). In addition, the SHG intensity increased with increasing particle size and a decreasing tendency was not observed, manifesting that SHG is phase-matchable at 1064 nm, which was also verified using the calculated chromatic dispersion curves.

Birefringence, as a key parameter to achieve phase-matching, is essential for NLO crystals. Therefore, in order to know the phase-matching capability of ABAF, we next investigated its birefringence. According to the refractive index calculated using first-principles calculations, birefringence of ABAF at 1064 nm is determined to be 0.03. Obviously, such a value is larger than that of most of the reported SHG-active boron phosphates and phosphates (see Table 1). Notably, this value is also comparable to those of several newly discovered bismuth- and/or lead-based NLO phosphates, namely, $A_3BBi(P_2O_7)_3$ (A = Rb, Cs; B = Pb, Ba) ($\Delta n$ = 0.025–0.03 at 1064 nm) which encompass highly distorted Bi–O and/or Pb–O polyhedra which easily induce an enhanced birefringence.[41]

It seems necessary to discuss the possible mechanism of birefringence enhancement observed in ABAF and we inferred that $[BO_3F]$ tetrahedra are mainly responsible for this. As shown in Table 1 and Fig. 3, those NLO crystals assembled with tetrahedra in which the central atoms are coordinated with all O atoms universally have smaller birefringence than those composed of tetrahedra in which the central atoms are coordinated with mixed O atoms and F atoms. This suggests that the all-oxygen-coordinated $AsO_4$ geometry in ABAF is probably not the leading contributing one to birefringence enhancements. Therefore, it seems that such improvements are possibly due to the $BO_3F$ tetrahedron. Actually, as described earlier, based on theoretical computation, the occurrence of F atoms in tetrahedral geometric anions is in favor of strengthening birefringence, and desirable improvements are indeed discovered in some NLO materials, such as $(NH_4)_2PO_3F$, and $NaNH_4PO_3F\cdot H_2O$ (Table 1). It should be mentioned that it is difficult to quantitatively describe the contribution of $BO_3F$ tetrahedra to birefringence. The related discussions are just based on the previous work and reasonable speculation.

## Optical property comparison

To more intuitively comprehend the key linear and nonlinear optical properties of ABAF, the SHG coefficient-, birefringence-, and SHG coefficient-birefringence plots of the recently discovered NLO crystals exclusively composed of nonπ-conjugated tetrahedral FBUs, are shown in Fig. S2† and 3, with deep-UV transparency window as the prerequisite. Firstly, the SHG

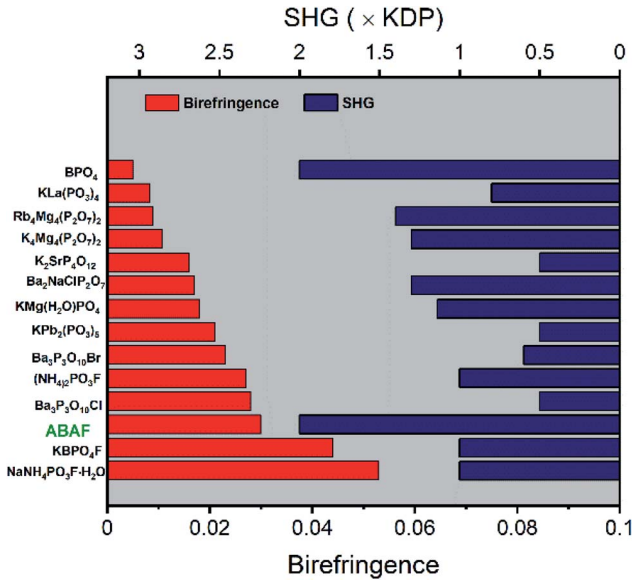


Fig. 3 The SHG coefficient and birefringence summarization for NLO crystals assembled with tetrahedral units with deep-UV transmittance as a prerequisite.

coefficient of most of these crystals lies below the 2 × KDP line, and only a few crystals, including $BPO_4$, $LiCs_2PO_4$, $LiRb_2PO_4$, and $Li_2BaSiO_4$ as well as ABAF can touch or exceed this line, indicating that ABAF has enhanced SHG response which is not only highly competitive to those crystals with SHG efficiency <2 × KDP, but also comparable with $BPO_4$, $LiCs_2PO_4$, $LiRb_2PO_4$, and $Li_2BaSiO_4$ (Fig. S2(a)†). Secondly, as displayed in Fig. S2(b),† most of these crystals have poor birefringence less than 0.02, and only a few crystals including ABAF have an improved birefringence, larger than 0.03. Therefore, in the cases of birefringence and SHG response, ABAF achieved a preferable balance among these NLO crystals (Fig. 3).

### Thermal stability

DTA and TG analysis of ABAF were also performed to know its thermal stability. As shown in Fig. S5,† in the DTA curve, a sharp endothermic peak was observed at 389 °C, and simultaneously ABAF started to lose mass in the TG curve, revealing that ABAF could be stable up to 389 °C and above this temperature it starts to thermally decompose to other phases. The thermal stability of ABAF is better than those of NLO crystals containing $NH_4$, such as $NH_4B_4O_6F$ (~300 °C) and $NH_4Be_2BO_3F_2$ (~350 °C).

### Structure–property relationships

We carried out first principles calculations by using the DFT method within the CASTEP package to help understand the intrinsic relationship between the structure and optical properties of ABAF (see Fig. S4†). The calculated band structure suggests that ABAF has a band gap of 4.93 eV, which is smaller than the experimental value of 5.9 eV. The band gap underestimation originated from the inherent limitation of the exchange and correlation functional in the DFT method. Therefore, to well match the experimental gap and accurately describe the optical properties, a "scissor" of 0.97 eV was used in our following calculations and analyses.

The density of states (DOS), including the total DOS and partial DOS projected onto specific atoms is plotted in Fig. S7.† We focus on the energy zones in the vicinity of the forbidden band (−10 to 17 eV), which account for most of the chemical bonding characteristics in the compound. It is clear that in the region, the electronic states of N-2s 2p and H-1s and B-2s 2p and O-2p together with F-2p, as well as As-4s 4p and O-2p are well overlapped, inferring the strong bonding interactions of N–H, B–O, B–F and As–O bonds in the system. The upper part of the VB (−5 to 0 eV) is dominated by O-2p and F-2p states, with a bit of As-4p and B-2p states mixed; while the lower part of CB (5–10 eV) is composed of the unoccupied As-4s 4p, O-2p and small amount of B-2p states. Since the optical properties of a material are mainly dependent on the electronic states on both sides of the forbidden band, it can be predicted that the optical properties of ABAF are intimately associated with $[BO_3F]$ and $[AsO_4]$ tetrahedra in the $[BAsO_4F]_\infty$ layers.

We next calculated the SHG coefficients. Among them, $d_{12}$ is the largest tensor whose absolute value is 1.25 pm $V^{-1}$ in the static limit. The magnitude of $d_{12}$ is about 3.2 times that of KDP ($d_{36}$ = 0.39 pm $V^{-1}$), consistent with the measured powder SHG effect (2 times that of KDP). To elucidate the inherent origin of the SHG response of ABAF, we further performed the SHG-weighted electron density (SHG-density) analysis for $d_{12}$, which can clearly disclose the SHG-contributed orbitals in the real space (Fig. 4): in the VB, the O-2p and F-2p nonbonding states in $AsO_4$ and $BO_3F$ tetrahedra dominate the SHG effect, and in the CB, the empty orbitals of O-2p and As-4s 4p contribute principally to the SHG effect. Based on the SHG-density analysis, we also calculated the contribution percentages to the SHG effect from the constituent groups, which are 63.01% for $AsO_4$, 32.96% for $BO_3F$ and 4.03% for $NH_4^+$. Obviously, the SHG-contribution of $NH_4^+$ is negligibly small. This can also be verified by the dipole moment calculations. The calculation was carried out by a bond-valence approach described previously.[42] The results are listed in Table S10.† Obviously, the net dipole moment direction of $BO_3F$ and $AsO_4$

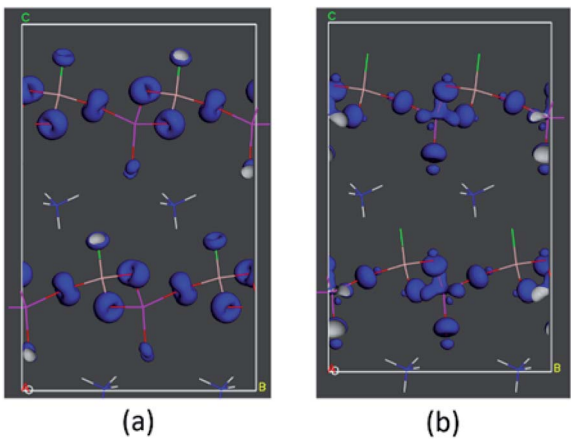


Fig. 4 SHG density map of the (a) VB and (b) CB.

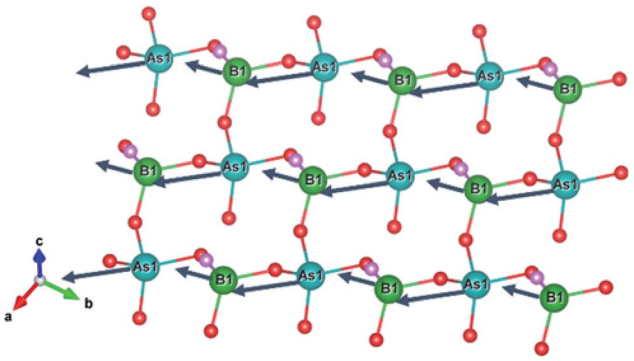


Fig. 5 The direction of net dipole moments of $BO_3F$ and $AsO_4$ tetrahedra.

pointed to the same direction (Fig. 5), suggesting their overlapping instead of cancelling out, which are favourable for the enhancement of the SHG effect. In addition, the magnitude of the net dipole moment for the $AsO_4$ tetrahedron is about 2.05 Debye, larger than that of $BO_3F$ (1.17 Debye), revealing that $AsO_4$ contributed more to the overall SHG effect than the $BO_3F$ group. Above all, it could be concluded that the cooperative interaction of $BO_3F$ and $AsO_4$ tetrahedra enables ABAF exhibit good nonlinear optical performances.

## Conclusions

In summary, the nonlinear optical and related properties of $NH_4BAsO_4F$ were investigated for the first time in this article. This material achieved improvements in key properties including birefringence and second-order nonlinearity. The study on structure–property relationships suggests that the 2D $[BAsO_4F]_\infty$ layers are mainly responsible for its optical properties. This work probably can provide some inspiration for identifying compounds with enhanced nonlinear optical properties by analysing structural features.

## Conflicts of interest

The authors declare no competing financial interest.

## Acknowledgements

This work was supported by the Strategic Priority Research Program of the Chinese Academy of Sciences (no. XDB20000000).

## Notes and references

1 P. Becker, *Adv. Mater.*, 1998, **10**(13), 979–992.
2 W. Yao, R. He, X. Wang, Z. Lin and C. Chen, *Adv. Opt. Mater.*, 2014, **2**(5), 411–417.
3 T. T. Tran, H. Yu, J. M. Rondinelli, K. R. Poeppelmeier and P. S. Halasyamani, *Chem. Mater.*, 2016, **28**(15), 5238–5258.
4 Y. Shen, S. Zhao and J. Luo, *Coord. Chem. Rev.*, 2018, **366**, 1–28.
5 M. Mutailipu, M. Zhang, Z. Yang and S. Pan, *Acc. Chem. Res.*, 2019, **52**(3), 791–801.
6 M. Mutailipu and S. Pan, *Angew. Chem., Int. Ed.*, 2020, **59**(46), 20302–20317.
7 P. S. Halasyamani and J. M. Rondinelli, *Nat. Commun.*, 2018, **9**(1), 1–4.
8 L. Kang, S. Luo, G. Peng, N. Ye, Y. Wu, C. Chen and Z. Lin, *Inorg. Chem.*, 2015, **54**(22), 10533–10535.
9 G. Shi, Y. Wang, F. Zhang, B. Zhang, Z. Yang, X. Hou, S. Pan and K. R. Poeppelmeier, *J. Am. Chem. Soc.*, 2017, **139**(31), 10645–10648.
10 Y. Wang, B. Zhang, Z. Yang and S. Pan, *Angew. Chem., Int. Ed.*, 2018, **57**(8), 2150–2154.
11 B. H. Lei, Z. Yang, H. Yu, C. Cao, Z. Li, C. Hu, K. R. Poeppelmeier and S. Pan, *J. Am. Chem. Soc.*, 2018, **140**(34), 10726–10733.
12 F. Pan, G. Shen, R. Wang, X. Wang and D. Shen, *J. Cryst. Growth*, 2002, **241**(1–2), 108–114.
13 X. Zhang, L. Wang, S. Zhang, G. Wang, S. Zhao, Y. Zhu, Y. Wu and C. Chen, *J. Opt. Soc. Am. B*, 2011, **28**(9), 2236–2239.
14 P. Yu, L. M. Wu, L. J. Zhou and L. Chen, *J. Am. Chem. Soc.*, 2014, **136**(1), 480–487.
15 S. Zhao, P. Gong, S. Luo, L. Bai, Z. Lin, C. Ji, T. Chen, M. Hong and J. Luo, *J. Am. Chem. Soc.*, 2014, **136**(24), 8560–8563.
16 L. Li, Y. Wang, B. H. Lei, S. Han, Z. Yang, K. R. Poeppelmeier and S. Pan, *J. Am. Chem. Soc.*, 2016, **138**(29), 9101–9104.
17 L. Li, Y. Wang, B. H. Lei, S. Han, Z. Yang, H. Li and S. Pan, *J. Mater. Chem. C*, 2017, **5**(2), 269–274.
18 S. Zhao, X. Yang, Y. Yang, X. Kuang, F. Lu, P. Shan, Z. Sun, Z. Lin, M. Hong and J. Luo, *J. Am. Chem. Soc.*, 2018, **140**(5), 1592–1595.
19 H. Yu, J. Young, H. Wu, W. Zhang, J. M. Rondinelli and P. S. Halasyamani, *Chem. Mater.*, 2017, **29**(4), 1845–1855.
20 B. Zhang, G. Han, Y. Wang, X. Chen, Z. Yang and S. Pan, *Chem. Mater.*, 2018, **30**(15), 5397–5403.
21 H. Wu, B. Zhang, H. Yu, Z. Hu, J. Wang, Y. Wu and P. S. Halasyamani, *Angew. Chem., Int. Ed.*, 2020, **59**(23), 8922–8926.
22 G. Han, Y. Wang, B. Zhang and S. Pan, *Chem.–Eur. J.*, 2018, **24**(67), 17638–17650.
23 J. Lu, J. N. Yue, L. Xiong, W. K. Zhang, L. Chen and L. M. Wu, *J. Am. Chem. Soc.*, 2019, **141**(20), 8093–8097.
24 A. Lieb and M. T. Weller, *Z. Anorg. Allg. Chem.*, 2009, **635**(12), 1877–1881.
25 G. Peng, N. Ye, Z. Lin, L. Kang, S. Pan, M. Zhang, C. Lin, X. Long, M. Luo, Y. Chen, Y. H. Tang, F. Xu and T. Yan, *Angew. Chem., Int. Ed.*, 2018, **57**(29), 8968–8972.
26 G. Yang, P. Gong, Z. Lin and N. Ye, *Chem. Mater.*, 2016, **28**(24), 9122–9131.
27 I. D. Brown and D. Altermatt, *Acta Crystallogr.*, 1985, **41**(4), 244–247.
28 S. K. Kurtz and T. T. Perry, *J. Appl. Phys.*, 1968, **39**(8), 3798–3813.
29 L. Qi, Z. Chen, X. Shi, X. Zhang, Q. Jing, N. Li, Z. Jiang, B. Zhang and M. H. Lee, *Chem. Mater.*, 2020, **32**(19), 8713–8723.

30 S. Zhao, P. Gong, S. Luo, L. Bai, Z. Lin, Y. Tang, Y. Zhou, M. Hong and J. Luo, *Angew. Chem., Int. Ed.*, 2015, **54**(14), 4217–4221.
31 M. Abudoureheman, S. Han, B. H. Lei, Z. Yang, X. Long and S. Pan, *J. Mater. Chem. C*, 2016, **4**(45), 10630–10637.
32 P. Shan, T. Sun, H. Liu, S. Liu, S. Chen, X. Liu, Y. Kong and J. Xu, *Cryst. Growth Des.*, 2016, **16**(10), 5588–5592.
33 P. Shan, T. Sun, H. Chen, H. Liu, S. Chen, X. Liu, Y. Kong and J. Xu, *Sci. Rep.*, 2016, **6**(1), 1–10.
34 S. Zhao, Y. Yang, Y. Shen, X. Wang, Q. Ding, X. Li, Y. Li, L. Li, Z. Lin and J. Luo, *J. Mater. Chem. C*, 2018, **6**(15), 3910–3916.
35 J. H. Jiang, L. C. Zhang, Y. X. Huang, Z. M. Sun, Y. Pan and J. X. Mi, *Dalton Trans.*, 2017, **46**(5), 1677–1683.
36 Y. Shen, S. Zhao, B. Zhao, C. Ji, L. Li, Z. Sun, M. Hong and J. Luo, *Inorg. Chem.*, 2016, **55**(22), 11626–11629.
37 J. Chen, L. Xiong, L. Chen and L. M. Wu, *J. Am. Chem. Soc.*, 2018, **140**(43), 14082–14086.
38 Z. Bai, L. Liu, L. Zhang, Y. Huang, F. Yuan and Z. Lin, *Chem. Commun.*, 2019, **55**(58), 8454–8457.
39 Z. Bai, C. L. Hu, L. Liu, L. Zhang, Y. Huang, F. Yuan and Z. Lin, *Chem. Mater.*, 2019, **31**(22), 9540–9545.
40 Y. Li, F. Liang, S. Zhao, L. Li, Z. Wu, Q. Ding, S. Liu, Z. Lin, M. Hong and J. Luo, *J. Am. Chem. Soc.*, 2019, **141**(9), 3833–3837.
41 Q. Ding, X. Liu, S. Zhao, Y. Wang, Y. Li, L. Li, S. Liu, Z. Lin, M. Hong and J. Luo, *J. Am. Chem. Soc.*, 2020, **142**(14), 6472–6476.
42 P. A. Maggard, T. S. Nault, C. L. Stern and K. R. Poeppelmeier, *J. Solid State Chem.*, 2003, **175**(1), 27–33.